OPEN ACCESS
IOP Publishing
Classical and Quantum Gravity
Class. Quantum Grav. **41** (2024) 117004 (14pp) https://doi.org/10.1088/1361-6382/ad407e

Note

New Generation of Superattenuator for Einstein Telescope: preliminary studies

A Bertocco[1], M Bruno[1], R De Rosa[1,2], L Di Fiore[1], D D'Urso[3,4], F Frasconi[5,*], A Gennai[5], L Lucchesi[5], M Refat[1], F Pilo[5], D Rozza[3,4], P Ruggi[6], V Sipala[3,4], I Tosta e Melo[3,4] and L Trozzo[1,*]

[1] Istituto Nazionale di Fisica Nucleare, Sez. Napoli, Strada Comunale Cinthia, Naples 80126, Italy
[2] Dipartimento di Fisica 'Ettore Pancini', Univesrtità degli Studi di Napoli Federico II, Strada Comunale Cinthia, Naples 80126, Italy
[3] Dipartimento di Scienze Chimiche, Fisiche, Matematiche e Naturali, Università degli Studi di Sassari, Piazza Università 21, Sassari 07100, Italy
[4] INFN Laboratori Nazionali del Sud, Via S. Sofia 62, Catania 95123, Italy
[5] Istituto Nazionale di Fisica Nucleare, Sez. Pisa, Largo Bruno Pontecorvo 3, Pisa 50126, Italy
[6] European Gravitational Observatory, Via E. Amaldi, Cascina (Pi) 50621, Italy

E-mail: franco.frasconi@pi.infn.it and lucia.trozzo@na.infn.it

Received 16 October 2023; revised 26 March 2024
Accepted for publication 18 April 2024
Published 8 May 2024

Abstract

Seismic noise and local disturbances are dominant noise sources for ground-based gravitational waves detectors in the low frequency region (0.1–10 Hz) limiting their sensitivity and duty cycle. With the introduction of high-performance seismic isolation systems based on mechanical pendula, the 2nd generation laser interferometric detectors have reached the scientific goal of the first direct observation of GW signals thanks to the extension of the detection bandwidth down to 10 Hz. Now, the 3rd generation instrument era is approaching, and the Einstein telescope giant interferometer is becoming a reality with the possibility to install the detector in an underground site where seismic noise is 100 times smaller than on surface. Moreover, new available technologies as well as the experience acquired in operating advanced detectors are key points to further extend the detection bandwidth down to 2 Hz with the possibility

* Authors to whom any correspondence should be addressed.

to suspend cryogenic payload and then mitigating thermal noise too. Here, we present a preliminary study devoted to improving seismic attenuation performance of the advanced VIRGO superattenuator in the low frequency region of about five orders of magnitude. Particular care has been carried on in analyzing the possibility to improve the vertical attenuation performance with a multi-stage pendulum chain equipped with magnetic anti-springs that is hung to a double inverted pendulum in nested configuration. The feedback control requirements and possible strategies to be adopted for this last element will be presented.

Keywords: seismic noise, seismic isolation, mechanical filters, interferometric detectors

1. Introduction

The first direct observation of a gravitational wave signal (GW150914) by using ground-based interferometric detectors, marked the starting point of a new era in the Universe study [1]. After that, more than 5 years of joint observation run by the LIGO and Virgo collaborations working as a single network with three interferometers based on the same working principle, has produced many scientific results [2]. The observation of a relevant number of stellar binary black-hole mergers has completely changed the previous expectation for a population of intermediate-mass black-holes and black-hole binary formation. Moreover, the simultaneous observation of binary neutron stars by GW instruments and space gamma-ray detectors, followed by the identification of the astronomical counterpart and consequent measurement of the EM afterglow using standard telescopes in IR, visible, UV, and x-ray frequency bands have opened the new research field of multi-messenger astrophysics [3]. The success of the modern GW detectors, based on the working principle of the Michelson interferometer with Fabry–Perot optical cavity along the two orthogonal arms, is the result of the wide technological developments lasted many decades. The pioneering cryogenic Weber resonant bar has been replaced by the development of a new concept of an interferometric detector with a laser source. This lead to the first idea of a broad frequency band instrument and then to the construction of the two LIGO detectors in the USA and the French–Italian VIRGO interferometer in the Pisa countryside (Italy). Today they represent, passing through different upgrade programs, the 2nd generation interferometers that finally observed GW signals on Earth. In the following paragraphs, we report the results of our preliminary studies on the detector sensitivity to technical and environmental noise sources. This is of great relevance in the frequency region below 10 Hz where the active feedback control of the detector introduces some disturbances and seismic noise represents an important limiting factor of the instrument performance [4]. A simulation model based on the experimental apparatus of the advanced VIRGO (AdV) interferometer and developed within the MATLAB commercial software has been used to this purpose, with the intent to optimize the instrument response in view of the Einstein telescope (ET) interferometer construction. In figure 1 a comparison between the AdV displacement sensitivity during the last data taking period (O3—observation run 3) and the design sensitivity of the ET giant interferometer is shown [5]. The frequency bandwidth of the 2nd generation detectors ranges from 10 Hz to 10 kHz, while for the 3rd generation ones, like ET, the goal is the improvement of the current sensitivity by about a factor 10 extending the observation bandwidth down to about 2–3 Hz. For the AdV detector this means that the required improvement with respect to the present experimental limits is more than 5 orders of magnitude [6] defining also important guidelines for future technologies to be implemented in the field.

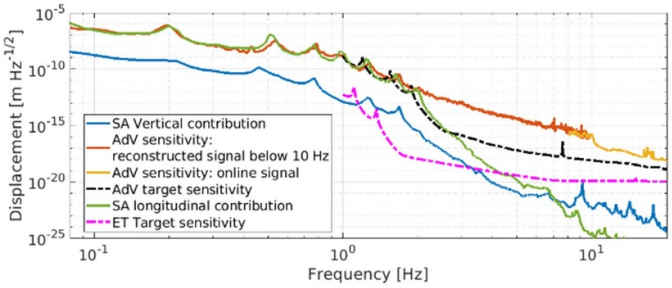

Figure 1. Displacement sensitivity of 2nd generation detector AdV compared with its design sensitivity and the ET target sensitivity.

2. New Generation of Superattenuators (NGSAs)

The modern GW detectors are based on a Michelson interferometer (ITF) with a LASER source and two Fabry–Perot optical cavities along the arms 3–4 km long each one. The experimental apparatus is formed by a complex mechanical structure, ground based, to support the delicate test masses, the mirrors, where the laser beam is reflected forward and backward. The structure adopted to isolate and suppress seismic noise transmitted to the test masses, is meant as fundamental element of the instrument so that to consider the test masses as free-falling bodies starting from a few Hz. To this purpose, a cascade of harmonic oscillators has been developed with the intention of having the mechanical structure act passively above a cut-off frequency, while the internal modes are confined to the low frequency range where active suppression is applied. The introduction of the superattenuator (SA) [6–8] as a hybrid system for filtering seismic noise and suspending the optical components of the advanced VIRGO interferometer is, today, a cornerstone of the present technology and the most performant seismic isolation system in the world. As shown in figure 2 the AdV superattenuator is conceived as a three-legs mechanical structure based on the working principle of an inverted pendulum (IP). Together with the filter on its top (called Filter 0) it has two fundamental roles: (i) it represents a pre-isolation stage starting from a few tens of mHz and (ii) it is used as a mechanical support for the suspension point of the filter chain. Moreover, thanks to the presence of a set of sensors (position sensors and acceleration sensors) and actuators, it is possible to actively dump the inner modes of the chain and to compensate the tidal effect applying small forces (of the order of a few Newtons). The total length of this structure, from the suspension point of the filter chain on Filter0 to the center of the mirror, is about 9 m.

Considering the same experimental lines mentioned above and thanks to the experience acquired in operating a so complex system to isolate the test masses from seismic noise, a project to develop a NGSAs has been elaborated with the goal to reach the target performance demanded by the ET interferometer. In this paper we consider two possible configurations as guidelines for the next generation of superattenuator. The first one represents the traditional solution, as detailed in the framework of the ET conceptual design [9, 10]. It consists of a longer version of the SA presently in operation on the AdV interferometer, with a three-legs Inverted Pendulum pre-isolator stage supporting a chain of mechanical filters and payload. With this configuration, the ET attenuation requirement can be achieved optimizing the mass distribution along the filters chain [11], improving the performance of the magnetic anti-spring system installed on each filter, and forming a multi-stage pendulum with all elements at the same relative distance. Even with this geometry the ET stringent requirements can be fulfilled

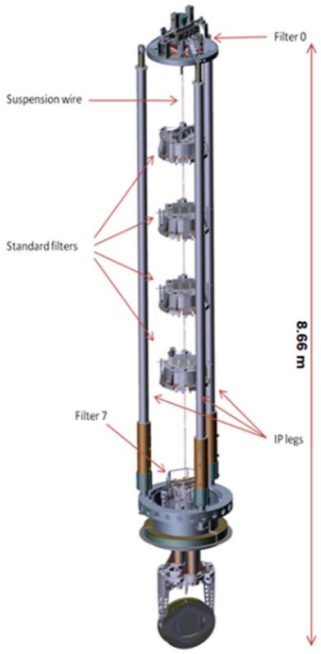

Figure 2. Technical drawing of the AdV Superattenuator. Together with the three legs structure of the inverted pendulum (ground connected through the bottom ring visible in this rendering), from the top to the bottom, are visible: the filter F0 (on the top of the platform), a chain of five mechanical filters, and the payload (marionette and mirror). Reproduced with permission from [6].

keeping the total length of the structure (from suspension point to mirror center) as small as 12 m.

The second and more innovative solution, is based on the use of two pre-isolators Inverted Pendulum in a Nested configuration (NIP) where the innermost one supports the traditional multistage pendulum chain and the payload (see figure 3). Here below we describe the results of a preliminary simulation campaign devoted to the optimization of some relevant parameters for this innovative approach. Our study is based on the possibility to reduce the total length of the mechanical structure within 10 m optimizing the mass distribution along the chain, reducing the crosstalk among different degrees of freedom and confining the mechanical modes below 1.5 Hz.

2.1. NIP-SA as a solution for the ET detector

The solution with a NIP as a pre-isolation stage offers evident advantages from the point of view of horizontal attenuation performance at the level of the test mass. With this geometry, our preliminary studies show that the total hight of the superattenuator could be maintained around 10 m fulfilling the seismic filtering performance for ET. In figure 3 is showed a 2D sketch layout of this superattenuator with NIP.

It consists of a first Inverted Pendulum (IP1), ground connected through its feet, from which a mechanical platform is hung and supporting a second pre-attenuation stage (IP2). On top of

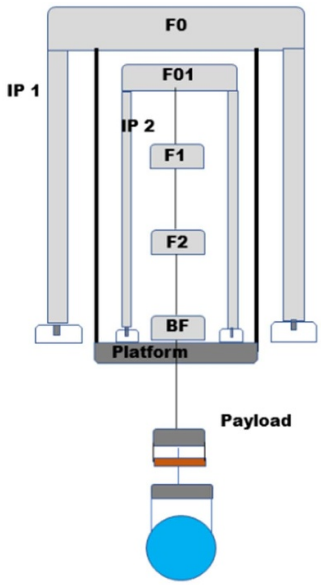

Figure 3. 2D sketch of the NIP-SA. All the isolation stages are visible going from the top to the bottom: the first pre-isolator (inverted pendulum-IP1 grounded connected through its feet), a second inverted pendulum-IP2, three passive mechanical filters, and the payload (last four stages).

the IP2, a chain of three passive filters (F1, F2, and BF) with the last four stages of a payload (for a total load of about 600 kg) [12] is suspended.

On the other hand we do not forget that a nested inverted pendulum has never put in operation within the mechanical structure of a Superattenuator. All this leads to many open questions about its stability, its automatic control, and the crosstalk among different degree of freedom as well as about the difficulty in the normal modes confinement below 1.5 Hz. For these reasons it is important to develop a detailed simulation model before starting a prototyping process.

3. Modeling the NIP-SA system

In this paragraph we pass through the key points of the simulation model of our superattenuator with two pre-isolators Inverted Pendulum in a nested configuration (NIP-SA) which represents the most complex geometry considered. The goal is the detailed analysis of its mechanical behavior, the characterization of the filter chain normal modes and cross-couplings, as well as verifying the stability of the structure and its performance.

The model is based on representing each mechanical element as a rigid body (mass) or an elastic element (wires, blades), whose transmission properties are kept in a matrix $\boldsymbol{Z}(\omega)$ called **impedance matrix** [6, 13–15].

3.1. NIP-SA overall impedance matrix

In the impedance matrix representation, a complex mechanical system is a collection of components linked in series or parallel, whose transfer function is obtained using the impedance matrix algebra. According to these rules, the impedance matrix of our model is evaluated by

combining the impedance matrices of two inverted pendulums, the suspension wires, and the masses. Passing through the description of the system reported in figure 3 (from the payload to the IP1), we connect the following impedances: Z_{pay}, Z_{chain}, Z_{w}, Z_{IP1}, Z_{PF}, Z_{IP2} and Z_{F_i} [6, 13, 14]. The Z_{chain} is obtained by connecting in series Z_{pay} with the standard filters (Z_{F_i} and Z_{BF},) through the impedance matrix representing the elastic element of the suspension wires (Z_{w}) as follows:

$$Z_{\text{chain}} = Z_3 \cdot Z_{\text{w},} \cdot Z_{\text{F01}} \tag{1}$$

where Z_3 is given by:

$$\begin{aligned} Z_1 &= Z_{\text{pay}} \cdot Z_{\text{w},} \cdot Z_{\text{BF}} \\ Z_2 &= Z_1 \cdot Z_{\text{w},} \cdot Z_{\text{F2}} \quad . \\ Z_3 &= Z_2 \cdot Z_{\text{w},} \cdot Z_{\text{F1}} \end{aligned} \tag{2}$$

From the filters chain to the IP1, the $\boldsymbol{Z_{SUS}}$ matrix, representing the overall suspension, is obtained by connecting in series Z_{chain}, Z_{IP2}, Z_{PF}, $Z_{\text{W}_{\text{PF}}}$, and Z_{IP1}. Here Z_{PF} and Z_{WPF}, represent the impedance of the mechanical platform and its suspension wires respectively, while Z_{SUS} matrix is used to calculate the transfer function from ground to test mass. The result of this computation provides a 12×12 complex matrix whose elements are the transfer functions for a selected d.o.f. of the system.

3.2. NIP-SA: preliminary transfer functions

Given the complexity and the dimension of the matrices, specific MATLAB code has been developed and used over the last twenty years for evaluating and improving the AdV seismic attenuators response [6, 8, 14]. This code, in combination with the mass distribution optimization approach given in the work [11], has been widely emploied to investigate the coupling terms among degrees of freedom and optimizing the NIP-SA performance by tweaking appropriate parameters like length, stiffness, and mass. In this section, **the longitudinal, tilt coupling**, and **the vertical** transfer functions for the following configurations have been calculated:

- **Case A**: a NIP-SA 8 m tall with a total mass of 2650 kg
- **Case B**: a NIP-SA 10 m tall with a total mass of 2650 kg
- **Case C**: a NIP-SA 10 m tall with a total mass of 3250 kg

The vertical transfer function is calculated considering four standard filters (F01, F1, F2, and BF) identical to those ones of the AdV SA [6–8]. In figures 4 and 5, the simulated transfer functions for the longitudinal d.o.f., tilt-coupling d.o.f. and completed with their zoom in the frequency region 0.8–3 Hz, are respectively shown. The TF value at 2 Hz is $6 \cdot 10^{-11}$ for all the configurations considered and for the longitudinal d.o.f. As detailed in section 5, this result represents a good achievement for our purposes. However, an improvement on the tilt-coupling parameter of a factor 16 at 2 Hz, is well visible passing from the configuration of the Case A to the configuration of the Case C ($2.5 \cdot 10^{-5}$ for Case A, $4.3 \cdot 10^{-6}$ for Case B and $1.5 \cdot 10^{-6}$ for Case C). Moreover, the simulation results obtained for the vertical transfer function of the three different configurations reported in the plots of figure 6, show that they are similar. The presence of a peak in the region 30–50 Hz puts in evidence a deteriorated response of the mechanical filters which can be mitigated with a new geometry of the magnetic anti-spring. To this purpose the optimization of a new cross-bar design equipped with rare earths permanent magnets is in progress, because the total weight of the structure (cross-bar mechanical structure and magnets) seems to be at the origin of the problem.

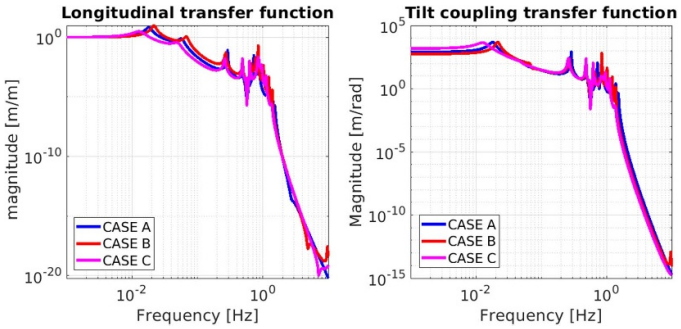

Figure 4. NIP-SA transfer function, from ground to suspended mass, longitudinal d.o.f (left panel) and tilt coupling (right panel).

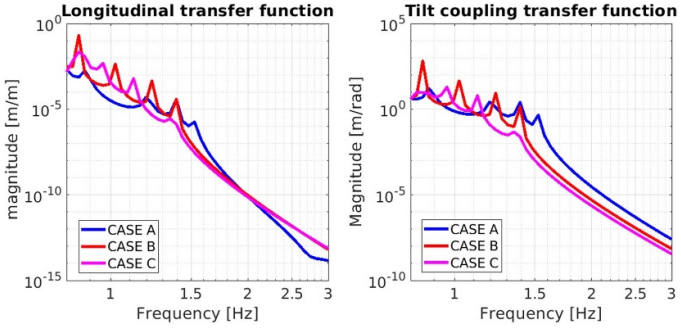

Figure 5. NIP-SA transfer function zooms of longitudinal d.o.f (left side) and tilt coupling (right side) as simulated for three different configurations. At 2 Hz, the longitudinal attenuation is about $6 \cdot 10^{-11}$, while tilt-coupling attenuation improves of a factor 16, changing from Case A to Case C.

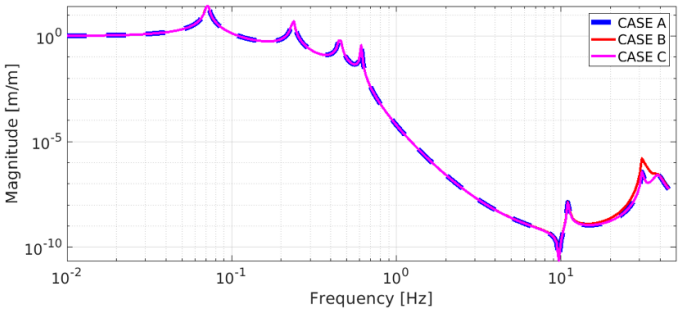

Figure 6. Vertical transfer function for three different configurations of the NIP-SA: a peak structure is visible in the frequency region 30–50 Hz.

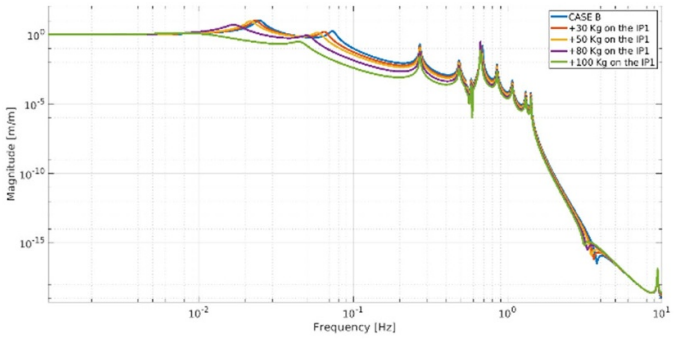

Figure 7. Transfer function of the IP1 for different ballast installed on its top stage and for the geometry of the Case B as detailed in the text. The different curves represent the response of the system when a ballast is used on the IP1 up to the instability of the system (curve labelled + 100 kg).

3.3. NIP-SA: potential instabilities condition

Exploring the instability of our NIP-SA, which is a typical non-degenerate mechanical system, it is possible to approach the problem heuristically by counting the number of modes visible in the transfer function plot in the frequency region below 100 mHz. Furthermore, being our system a composite one with two inverted pendulums, it is expected to show two resonances (one for each IP). Under this assumption and without losing generality, one might try to give a heuristic stability criterion for the NIP-SA: it is stable if both modes are present below 100 mHz, while it is unstable if the lower value is moved to the flat region of the spectrum[7]. Adding some ballast, indeed, it is possible to move the IP frequency down to its instability in accordance with the equations reported in the endnote below and detailed in [16, 17]. In figure 7 is reported the transfer functions obtained with our simulation model (Case B) and with different ballast on top of the IP1 evaluating the system stability.

The curves shown in figure 8, instead, are the transfer functions of our system when the ballast is installed on top of the IP2. This has been done with the intent to evaluate the stability of the system as in figure 7.

However, the optimization and the stability of the NIP-SA structure will be studied in experimental way avoiding problems of any origin and finding the right compromise in the ballast distribution (on IP1 and on IP2).

4. Seismic noise measured at Sos Enattos site

Seismic noise in underground and surface locations depends on the proximity to the coast, urban areas, and their geological history morphology. At frequencies $f > 1$ Hz, the amplitude of the seismic spectrum is associated with human activities and with drastic weather changes. Moving from surface to underground, it is possible to observe that the atmospheric perturbation influence is minimal: the environmental conditions are more stable and, therefore, seismic

[7] In the frequency domain the behavior of the IP is governed by the equation $f_{\mathrm{IP}} = \frac{1}{2\pi}\sqrt{\left(\frac{k}{m} - \frac{g}{L}\right)}$ and, as a consequence, the stability condition for this mechanical structure is fixed by the mathematical relation $\left(\frac{k}{m} - \frac{g}{L}\right) > 0$ where m is the ballast on top of IP, k is the total stiffness of the three legs with flex joints and L their length.

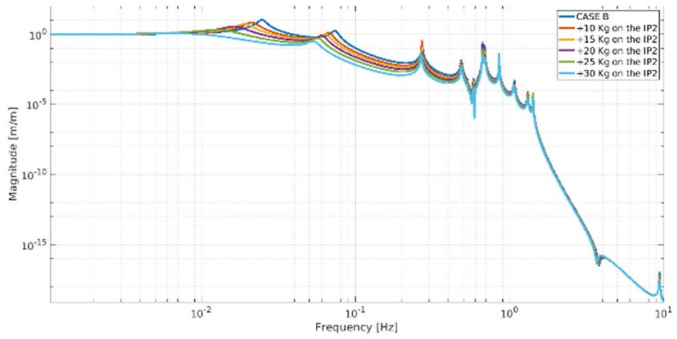

Figure 8. Transfer function of the IP2 for different ballast installed on its top stage and for the geometry of the Case B as detailed in the text. The different curves represent the response of the system when a ballast is used on the IP2 up to the instability of the system (curve labelled + 30 kg).

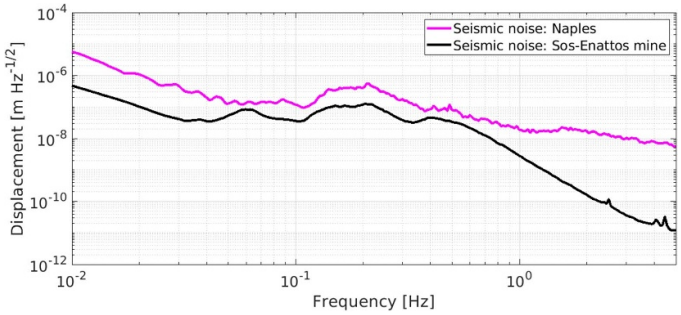

Figure 9. Spectral density of seismic noise displacement measured at laboratory of Experimental Gravitation in Naples, compared to that one measured at Sos Enattos former mine.

noise is attenuated by about a factor of 100 [18, 19] with respect to the surface. This has been put in evidence in figure 9, where the horizontal spectral seismic noise profiles measured at Naples and at the Sos Enattos former mine, are plotted. In particular, at 2 Hz seismic noise value associated to Naples site is $10^{-8}\frac{\mathrm{m}}{\sqrt{\mathrm{Hz}}}$, while that one associated the Sos Enattos former mine is $8\cdot 10^{-11}\frac{\mathrm{m}}{\sqrt{\mathrm{Hz}}}$. Low seismic noise level, geological stability, as well as the distance from industrial activities of the Sos Enattos's site represent the most appealing features of this area to be considered one of the best candidates to host the construction of the Einstein telescope (ET).

4.1. Sos Enattos site: ground tilt lower limit estimation

Despite the efforts performed by different experimental groups [20, 21] in the development of a suited sensor for high precision ground-tilt measurements, we do not have any experimental measurements supporting our simulation model investigation, and we can only give a lower limit evaluation of it by using the following empirical formula:

$$\alpha_0 = \frac{\omega}{v}\cdot x_0 \tag{3}$$

where v and x_0 are the seismic waves' speed and the longitudinal spectral density of the ground displacement, respectively. Assuming the value for v to be 3000 m s^{-1} and for x_0 to be $8 \cdot 10^{-11} \frac{\mathrm{m}}{\sqrt{\mathrm{Hz}}}$, the estimated lower limit of the α_0 spectral density at 2 Hz is about $3 \cdot 10^{-13} \frac{\mathrm{rad}}{\sqrt{\mathrm{Hz}}}$.

5. NIP-SA performance: projection on the ET LF sensitivity

A good method in determining whether a seismic isolation system is compliant with GW detector requirements is to measure how much seismic noise is transmitted to the test mass. The purpose of this section is to determine the amplitude spectral density of residual motion for a test mass suspended through the NIP-SA, as described in section 3 and virtually installed in the Sos Enattos site.

5.1. Longitudinal and tilt coupling contributions

The residual motion of the test mass of our NIP-SA (response of the system), can be evaluated by filtering the longitudinal seismic profile reported in figure 9 and using the ground tilt estimated in paragraph 4.1. This has been done through the transfers function of the NIP-SA suspensions, plotted in figures 4 and 5, as follows:

$$x_{\mathrm{TM}_1} = \mathrm{TF}_{xx} \cdot x_0 \tag{4}$$

$$x_{\mathrm{TM}_2} = \mathrm{TF}_{x\alpha} \cdot \alpha_0. \tag{5}$$

In figure 10 the residual motion of the test mass along the longitudinal degrees of freedom is drawn (left panel), while a zoom of the region 0.8–3 Hz (right panel) completes the estimation for the three different configurations. All the results are compared to the ET sensitivity curve (dotted line). The residual motion of the test mass at 2 Hz reaches the spectral density value of $5 \cdot 10^{-21} \frac{\mathrm{m}}{\sqrt{\mathrm{Hz}}}$, which is more than two orders of magnitude lower than the ET design sensitivity ($10^{-18} \frac{\mathrm{m}}{\sqrt{\mathrm{Hz}}}$).

The tilt contribution within our simulation model has been evaluated by using the equation (3) and the seismic spectral density (x_0) as measured at Sos Enattos site (see black curve plotted in figure 9). As previously anticipated, this is considered a lower limit because no experimental measurements are available. In table 1 is summarized the results obtained at 2 Hz. This is the contribution to the residual motion of the test mass due to the ground tilt calculated with equation (5) and for three different configurations of NIP-SA as described in the text.

In CASE A, the tilt coupling is eight times higher than the ET sensitivity, in CASE B, it is approaching the ET target value, while in CASE C, it is two times lower than the nominal value of the sensitivity. According to these values we can preliminarily conclude that the tilt contribution may limit the detector sensitivity.

5.2. Vertical contribution

Due to the Earth curvature the coupling term, α_{grav}, between longitudinal and vertical direction is not negligible. Indeed, on about 10 km, the expected value of α_{grav} is about $3 \cdot 10^{-3}$.

Assuming this value, and neglecting structural imperfection on the system, the estimation of the residual motion of the test mass due to the vertical contribution can be calculated as:

$$x_{\mathrm{TM}_3} = \alpha_{\mathrm{grav}} \cdot \mathrm{TF}_{yy} \cdot y_0. \tag{6}$$

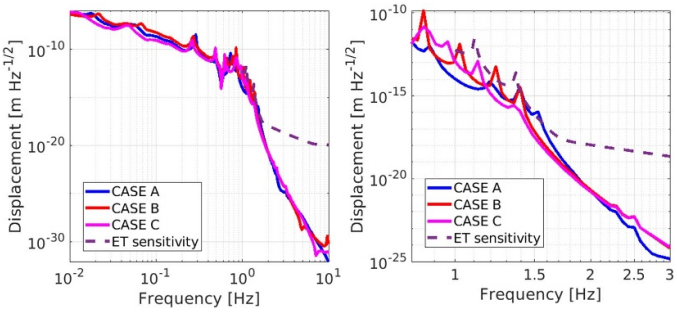

Figure 10. NIP-SA: expected residual motion of the test mass along the longitudinal degrees of freedom and due to the Sos Enattos seismic noise as represented by the black curve of figure 9. On the right-side panel, a zoom of the frequency region 0.8–3 Hz is shown.

Table 1. Expected residual motion of the test mass due to the ground-tilt contribution as estimated in section 4.1.

CASE A	$8 \cdot 10^{-18} \frac{\mathrm{m}}{\sqrt{\mathrm{Hz}}}$
CASE B	$10^{-18} \frac{\mathrm{m}}{\sqrt{\mathrm{Hz}}}$
CASE C	$4.5 \cdot 10^{-19} \frac{\mathrm{m}}{\sqrt{\mathrm{Hz}}}$

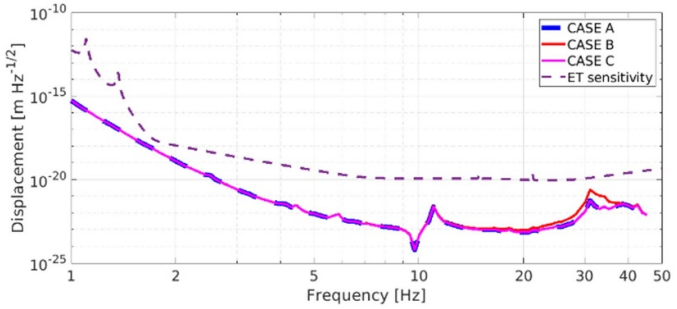

Figure 11. NIP-SA zoom of the expected residual motion of the test mass due to the vertical ground displacement in the region 1–50 Hz. In the region 1–3 Hz, the test mass displacement is about one order of magnitude below the ET sensitivity curve. In the range 5–20 Hz, the test mass displacement is more than two orders of magnitude below the ET sensitivity. Around 30 Hz, a mechanical resonance of the standard filters reaches the value of $5 \cdot 10^{-19} \frac{\mathrm{m}}{\sqrt{\mathrm{Hz}}}$.

In figure 11 is plotted a zoom of the residual motion for the test mass due to the vertical ground displacement in the frequency region 1–50 Hz for the three configurations considered. In this plot is superimposed the ET sensitivity curve (dotted line) for comparison purpose: the spectral density at 2 Hz is of the order of $10^{-19} \frac{\mathrm{m}}{\sqrt{\mathrm{Hz}}}$, providing a safety factor of 10 with respect to the ET demand.

Around 30 Hz, the presence of a mechanical resonance due to the crossbar of the standard filters, deteriorates the system response. For this reason, within our experimental program an important activity will be devoted to re-designing the filter crossbar and the magnetic anti-spring: they seem to be at the origin of the problem.

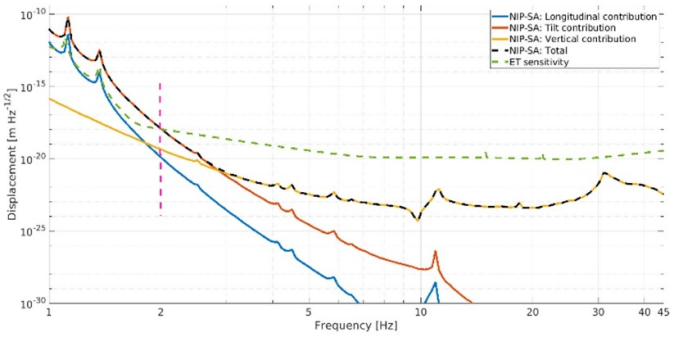

Figure 12. Expected residual motion of the test mass for the NIP-SA studied (Case B). Different contributions to the complete system response (see dotted curve labelled NIP-SA Total) are compared with the ET sensitivity (dotted green curve). A vertical dotted line at 2 Hz is marked in this plot as a reference value for all the studies carried out with this simulation activity.

As a general result of our studies, in figure 12 is plotted the expected residual motion of the test mass in the NIP-SA configuration for Case B. The different contributions (longitudinal—blue line, tilt—red line and vertical—yellow line) and the total response of the system are reported together with the ET target sensitivity (dotted green line).

6. Conclusions

In this paper we have summarized the preliminary results of our simulation studies around a NGSA for ET interferometer to be installed within the Sos Enattos mine. The used model is based on the Advanced VIRGO superattenuator where a two stage pre-isolator Inverted Pendulum in a Nested configuration (NIP) has been included as an innovative element. We demonstrated that adopting this configuration, the residual motion of the test mass is roughly two orders of magnitude lower than the ET target sensitivity along the longitudinal direction. Moreover, our study put in evidence that the cross-coupling between tilt and longitudinal direction, could be a potential problem whether a fine-tuning of the mechanical parameters is not performed in an accurate way. This is of great importance in view of obtaining the best performance of the new Superattenuators for next generation of GW detectors. This is also confirmed by the detailed evaluation of the vertical mechanical transfer function from which we inferred the need to re-designing the mechanical crossbar and the anti-spring system with the intent of improvig the passive filtering performance of each element of the multi-stage pendulum.

Data availability statement

All data that support the findings of this study are included within the article (and any supplementary files).

Acknowledgments

This work was partially supported by the Grant 'PRIN_2017 SYRTCN' from Ministero dell'Università e della Ricerca. Università degli Studi di Sassari with 'Fondo di Ateneo per la ricerca 2019' and 'Fondo di Ateneo per la riceca 2020'.

Conflict of interest

The authors declare not conflict of interest.

Funding

This research receveing not exsternal funding.

Computer program

The simulation code has been developed within MATLAB software.

ORCID iDs

R De Rosa https://orcid.org/0000-0002-4004-947X
L Di Fiore https://orcid.org/0000-0001-6296-1526
F Frasconi https://orcid.org/0000-0003-4204-6587
L Trozzo https://orcid.org/0000-0002-8803-6715

References

[1] Abbot B *et al* 2016 Observation of a gravitational wave from a binary black-hole merger *Phys. Rev. Lett.* **116** 061102
[2] Abbot B *et al* 2017 GW170814: a three-detector observation from a binary black-hole coalescence *Phys. Rev. Lett.* **119** 141101
[3] Abbot B *et al* 2017 GW170817: observation of a gravitational wave from a binary neutron star inspiral *Phys. Rev. Lett.* **119** 161101
[4] Aman F *et al* 2020 Site selection criteria for the Einstein telescope *Class. Quantum Grav.* **31** 105016
[5] Hild S *et al* 2011 Sensitivity studies for third generation gravitational waves observatories *Class. Quantum Grav.* **28** 094013
[6] Trozzo L 2018 Low frequency optimization and performance of advanced virgo seismic isolation system *PhD Thesis* University of Siena
[7] Ballardin G *et al* 2001 Measurement of the Virgo Superattenuator performance for seismic noise suppression *Rev. Sci. Instrum.* **72** 3643–52
[8] Acernese F *et al* 2010 Measurements of Superattenuator seismic isolation by Virgo interferometer *Astropart. Phys.* **33** 182–9
[9] Abernathy M *et al* 2011 Eistein telescope conceptual design (available at: https://tds.virgo-gw.eu/?call_file=ET-0106C-10.pdf) (Accessed June 2011)
[10] Punturo M *et al* 2020 Design report update 2020 for the Einstein telescope (available at: https://tds.virgo-gw.eu/?call_file=ET-0106C-10.pdf)
[11] Bove A, Fiore L D, Calloni E and Grado A 1997 Optimization of multi-pendular seismic suspensions for interferometric gravitational-wave detectors *Europhys. Lett.* **40** 601–6
[12] Majorana E 2022 private communication
[13] Vicerè A and Cella G 2001 Joining together different TFs private communication
[14] 2009 Modelling a multi-pendulum suspension (available at: https://tds.virgo-gw.eu/ql/?c=6714)

[15] Landau L 1975 *Theory of Elasticity* (Pergamon)
[16] Losurdo G *et al* 1999 An inverted pendulum preisolator stage for the VIRGO suspension system *Rev. Sci. Instrum.* **70** 2507–15
[17] Frasconi F and Rapagnani P 2014 *Advanced Interferometers and the Search for Gravitational Waves, Lectures from the First VESF School on Advanced Detetctors for Gravitational Waves* ed M Bassan (Springer) *Cap. 7* pp 193–224
[18] Naticchioni L *et al* 2014 Microseismic studies of an underground site for a new interferometer gravitational waves detector *Rev. Sci. Instrum.* **91** 09504
[19] Di Giovanni M *et al* 2021 A seismological study of the Sos Enattos area—the Sardinia candidate site for the Einstein Telescope *Seismol. Res. Lett.* **92** 352–64
[20] Venkateswara K, Hagedorn C A, Turner M D, Arp T and Gundlach J H 2014 A high-precision mechanical absolute-rotation sensor *Rev. Sci. Instrum.* **85** 015005
[21] Allocca A *et al* 2021 Picoradiant tiltmeter and direct ground tilt measurements at the Sos Enattos site *Eur. Phys. J.* **136** 1069